BURST PREDICTIONS OF HIGH PRESSURE PIPELINES WITH AXIAL FLAWS USING LOCAL CRITERIA

Claudio Ruggieri, claudio.ruggieri@usp.br
Fernando Dotta, fdotta@gmail.com
Department of Naval Architecture and Ocean Engineering, PNV-EPUSP
University of São Paulo, São Paulo, SP 05508–900, Brazil

Abstract *– This work extends a micromechanics approach based upon the computational cell methodology incorporating the Gurson model and the CTOA criterion to describe ductile crack extension of longitudinal crack-like defects in high pressure pipeline steels. The analyses demonstrate the effectiveness and limitations of both approaches to describe crack growth response and to predict the burst pressure for the tested pipes. While the CTOA criterion still appears to have limited applicability to predict ductile cracking behavior for the pipe specimens, the cell model predictions show good agreement with experimentally measured burst pressures.*

Keywords*: ductile tearing, burst pressure, R-curve, Gurson model, CTOA criterion*

1. INTRODUCTION

The accurate prediction of the failure pressure in damaged pipelines remains a key issue for the safety assessment of high pressure piping systems, including onshore and offshore facilities. Conventional failure criteria for longitudinal crack-like defects in pipelines (*e.g.*, blunt corrosion, inclusions, weld flaws, etc.) are derived based upon a simple fracture mechanics analysis for planar or crack-like flaws. Such procedures are calibrated by extensive burst testing of pipes containing machined cracks conducted on low-to-moderate strength structural steels (API Grades X52 and X60) [1] . While these acceptance criteria for linepipe defects clearly simplify integrity analyses of in-service piping components, they essentially reflect a limit-load solution for a blunted axial crack in a pressurized vessel or pipe. Moreover, these integrity assessment procedures assume failure criteria which do not necessarily reflect the actual failure mechanism (such as, for example, stable crack growth prior to final failure) nor do they address specific requirements for high grade pipe steels currently used. For these cases, failure assessments may be overly conservative or provide significant scatter in their predictions, which lead to unnecessary repair or replacement of in-service pipelines [2].

For high toughness pipeline steels, the material failure (leakage or sudden rupture) is most often preceded by large amounts of slow, stable crack growth. Under sustained ductile tearing of a macroscopic crack, large increases in the load-carrying (pressure) capacity for the flawed piping component are possible beyond the limits given by conventional elastic and elastic-plastic (stationary crack) analysis. Analytical methods for defect assessment in ductile materials generally employ the J-integral fracture parameter [3] to characterize the significant increase in toughness over the first few millimeters of stable crack extension (Δa). These methods rely direct application of crack growth resistance (J-Δa) curves (also often termed R-curves) measured using small, laboratory specimens to the surface defects in pressure vessels and pipelines [4-5]. However, laboratory testing of fracture specimens to measure resistance curves consistently reveals a marked effect of absolute specimen size, geometry, relative crack size (a/W) and loading mode (tension *vs*. bending) on R-curves. Consequently, advanced methodologies for fracture assessments of pipelines must include robust procedures to transfer fracture resistance data measured using small laboratory specimens to structural piping components in engineering applications.

This work extends a micromechanics approach based upon the computational cell methodology incorporating the Gurson model [6-7] and a deformation-based approach using the CTOA criterion [8,9] to describe ductile crack extension of longitudinal crack-like defects in high pressure pipeline steels. Laboratory testing of an API 5L X60 steel at room temperature using standard, deeply cracked fracture specimens provides the data needed to measure the crack growth resistance curve and to calibrate the Gurson and the CTOA parameters for this material. A central focus of the paper is the application of the cell methodology and the CTOA criterion to predict experimentally measured burst pressures for thin-walled gas pipeline containing longitudinal cracks. The experimental program includes precracked pipe specimens with 508 mm (20 inches) O.D. and 219 mm (8 5/8 inches) O.D. with varying crack depth to thickness ratios (a/t). Plane-strain computations are conducted on detailed finite element models for the pipe specimens to describe crack extension with increased pressure. The

numerical simulations demonstrate the effectiveness and limitations of both approaches to describe crack growth response and to predict the burst pressure for the tested pipes. While the CTOA criterion still appears to have limited applicability to predict ductile cracking behavior for the pipe specimens, the cell model predictions of the ductile response for the pre-cracked pipes show good agreement with experimentally measured burst pressures.

2. OVERVIEW OF NUMERICAL MODELING FOR STABLE CRACK GROWTH

2.1 Computational Cell Approach

Xia and Shih (X&S) [10] proposed an engineering approach based upon damage mechanics to predict *R*-curves for cracked configurations under ductile regime. Material separation occurs through a local fracture mechanism described by the micro-mechanics parameters D, which defines the thickness of the computational cell layer (on which Mode I growth evolves – Fig. 1) and the initial cell porosity, f_0, which roughly represents the actual metallurgical features of the material. Progressive void growth and subsequent macroscopic material softening in each cell are described by a constitutive model for dilatant plasticity given by Gurson [6] and Tvergaard [7] (GT) in the form

$$\left(\frac{\sigma_e}{\overline{\sigma}}\right)^2 + 2q_1 f \cosh\left(\frac{3q_2\sigma_m}{2\overline{\sigma}}\right) - \left(1 + q_3 f^2\right) = 0 \qquad (1)$$

where σ_e denotes the effective Mises (macroscopic) stress, σ_m is the mean (macroscopic) stress, $\overline{\sigma}$ is the current flow stress of the cell matrix material and f defines the current void fraction. Here, factors q_1, q_2 and $q_3 = q_1^2$ improve the model predictions for periodic arrays of cylindrical and spherical voids.

The GT yield function in Eq. (1) does not model realistically the rapid loss of stress capacity for larger void fractions nearing coalescence levels, nor does the model create new traction free surfaces to represent physical crack extension. In the present work, the evolution of stress within cells follows the original constitutive model of GT in Eq. (1) until $f = f_E$, where f_E denotes the critical volume fraction which typically has a value of ≈ 0.15. The final stage of void linkup with the macroscopic crack front then occurs by reducing the remaining stresses to zero in a prescribed manner. Tvergaard [7] refers to this process as the element extinction or vanish technique. When f in the cell incident on the current crack tip reaches a critical value, f_E, the computational procedure removes the cell thereby advancing the crack tip in discrete increments of the cell size. The equivalent nodal forces associated with the remaining stresses are released over a specified number of subsequent load steps, denoted as N_{rs}; the number of release steps is usually assigned a value of 10 in typical numerical analyses. It is beyond the scope of this brief article to address a full description of the computational cell methodology and the calibration procedure of the key parameters D and f_0. Interested readers are referred to the works of Xia and Shih [10], Ruggieri and Dodds [11] and Dotta and Ruggieri [13].

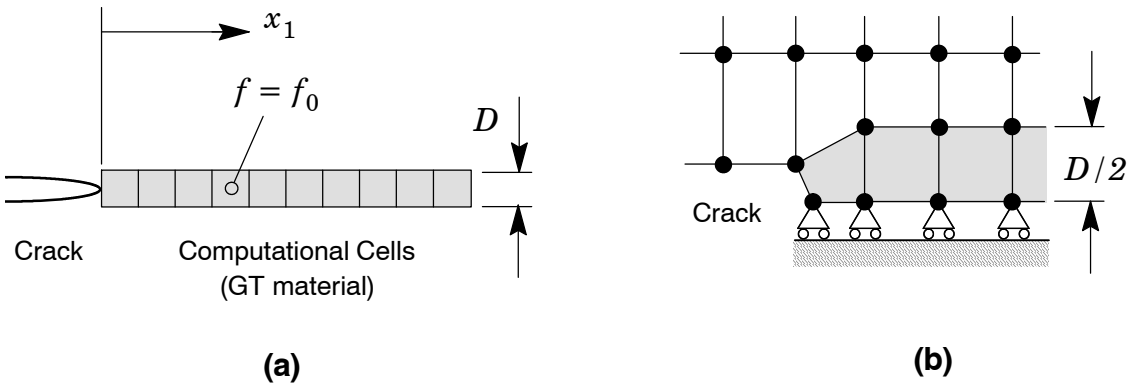

Figure 1 *Computational cell model for ductile tearing.*

2.2 CTOA Approach

Crack growth modeling approaches based upon macroscopic levels of deformation, such as J, CTOD or CTOA, retain contact with traditional fracture mechanics and provide a suitable framework to describe crack extension and instability during

the fracture process. In particular, models based on the CTOA concept attains particular relevance here as it provides a viable and convenient growth criterion for low constraint crack configurations such as fracture specimens and structural components made of thin materials [19-21]. CTOA-controlled crack growth operates by advancing the crack front a prescribed distance when the CTOA reaches a critical value, θ_c. A key assumption of the methodology lies in the adoption of a constant value of CTOA during stable crack growth. A number of experimental observations (see review by Newman et al. [21]) support the use of a constant CTOA from the onset of ductile tearing in numerical analyses of crack extension for ductile materials.

Figure 2 provides the essential features of the CTOA approach to describe ductile crack growth in a 2-D finite element setting. Figure 2(a) shows the deformed mesh of the upper-half plane before crack advance by node release. Symmetry conditions are enforced along the crack plane. Nodes unconstrained on the crack plane define the crack front whereas constrained nodes define the remaining ligament. The crack tip node and the nearest unconstrained node to the crack tip defines the two points required to calculate the local CTOA value. Crack extension occurs when the local opening angle computed at a crack front node reaches the critical CTOA-value. However, two critical CTOA-values for growth need to be specified: (1) the initiation angle, θ_I, which controls crack extension over the near-tip blunting region defined by the node on the initial crack tip and (2) the release angle, θ_R, which controls stable crack growth over the remaining nodes defining the crack ligament. Previous experimental and numerical studies [16-21] support the adoption of a higher value for the critical CTOA at crack initiation. A node release technique illustrated in Fig. 2(b) removes the constraint in the direction normal to the crack plane for the current crack-tip node. Similarly to the cell extinction procedure adopted in the previous methodology, the corresponding node reaction is reduced gradually to zero in subsequent load increments, N_{rs}, to avoid numerical difficulties. Further details on the numerical implementaion of the CTOA approach are provided by Gullerud et al. [19].

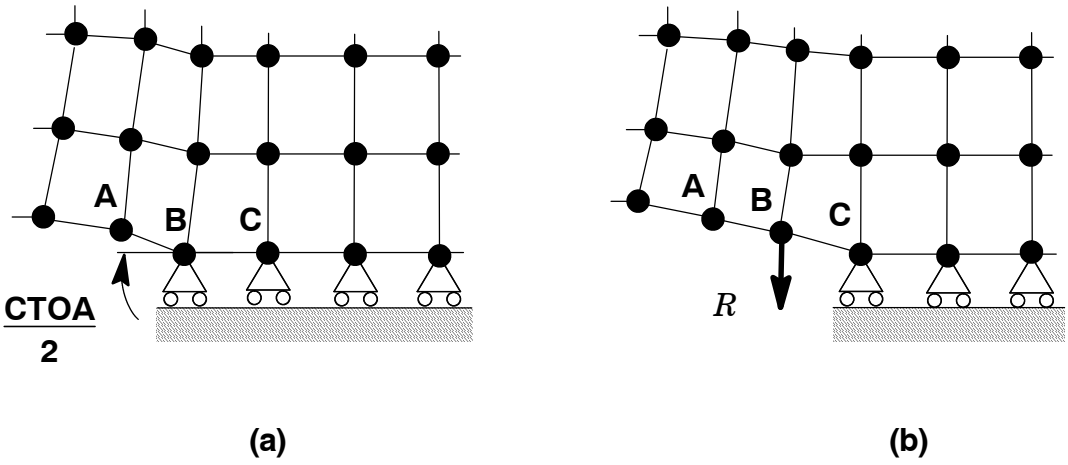

Figure 2 *Modeling of crack extension based upon CTOA.*

2.3 Computational Procedures

The finite element code WARP3D [12] provides the numerical solutions for the plane-strain analyses reported here. Key features of the code employed in this work include: (1) the GT and Mises constitutive models implemented in a finite-strain setting, (2) cell extinction using the traction-separation model, (3) automatic load step sizing based on the rate of damage accumulation, and (4) evaluation of the J-integral using a domain integral procedure.

Figure 3(a) shows the finite element model constructed for the plane-strain analyses of the 0.5-T C(T) specimen ($B = 13$ mm) with $a/W = 0.5$; this specimen was employed to measure the R-curve for the API X60 steel. Symmetry conditions permit modeling of only one-half of the specimen with appropriate constraints imposed on the remaining ligament. The half-symmetric model has one thickness layer of 1078 8-node, 3-D elements with plane-strain constraints imposed ($w = 0$) on each node. To simulate ductile crack extension, the finite element mesh contains a row of 130 computational cells along the remaining crack ligament ($W - a$) in a similar arrangement as shown in Fig. 1.

Figure 3(b) shows the finite element model constructed for the plane-strain analyses of the longitudinally cracked pipe with external diameter, $D_e = 20$ in (508 mm), and an internal crack with depth, a, of 7 mm made of API X60. The half-symmetric model has one thickness layer of 1171 8-node, 3-D elements with plane-strain constraints ($w = 0$) imposed on each node. Here, the finite element mesh contains a row of 88 computational cells along the remaining crack ligament ($t - a$).

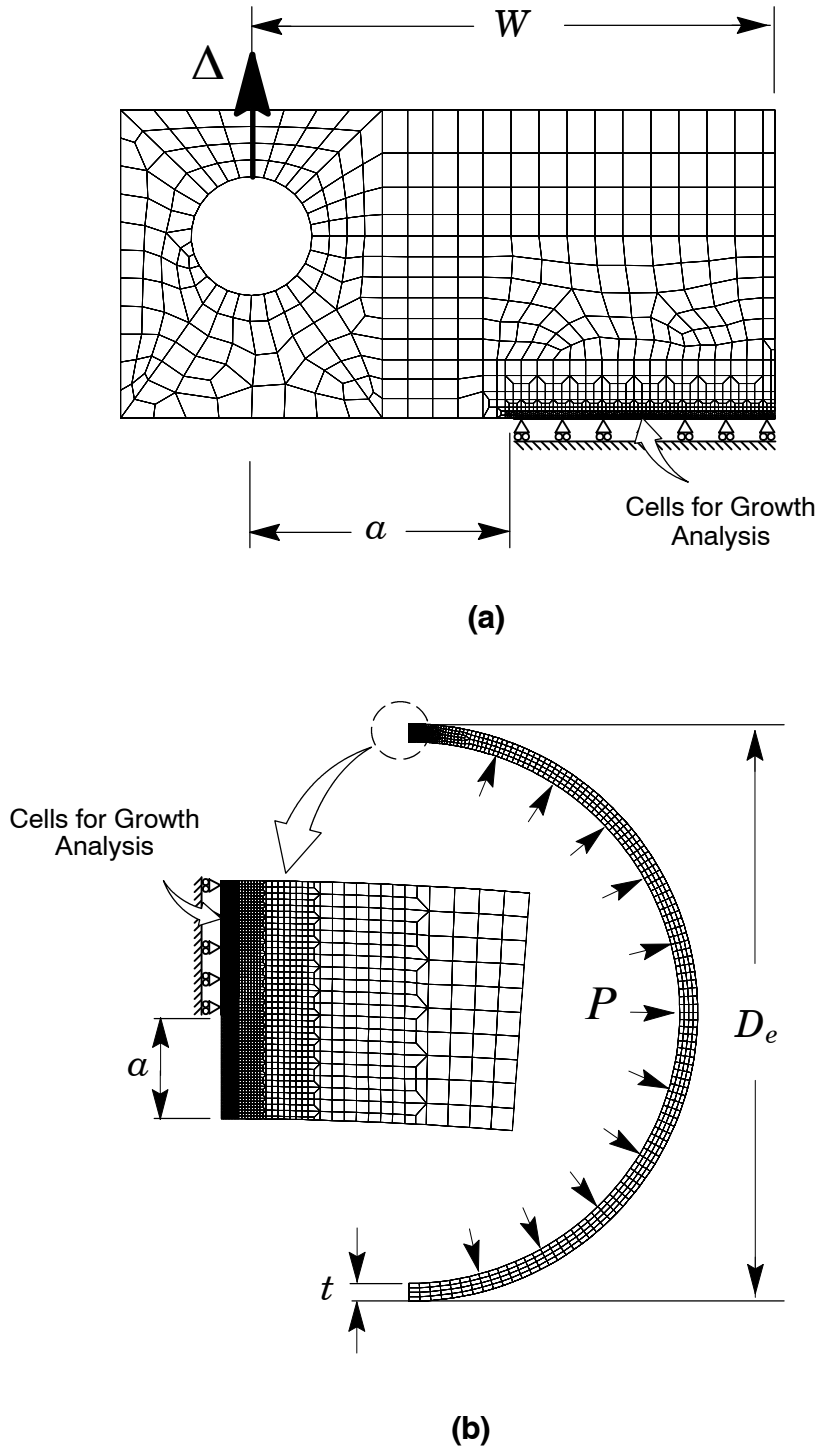

Figure 3 *Finite element models employed in the numerical analyses: a) plane-strain model of 0.5-T C(T) specimen with a/W = 0.5; b) plane-strain model of 20" O.D. pipe specimen with internal crack of 7 × 140 mm.*

3. CALIBRATION OF GT and CTOA PARAMETERS

A key step in the procedure to predict bust pressure for the precracked pipe specimens lies in the choice of the GT and CTOA parameters which govern the ductile response for the tested materials. Comparisons between predicted and experimentally measured fracture behavior (as described by the *R*-curves) for deep notch C(T) specimens enable a convenient and yet accurate calibration of these parameters. These calibrated values are then applied in similar analyses to predict ductile extension in the precracked pipe specimens.

Laboratory testing of standard compact tension C(T) specimens (side-grooved) extracted from pipe specimens in the TL position provided the tearing resistance curves (J *vs.* Δa) at room temperature (20°C) to calibrate the micromechanics parameters for the tested API X60 steel [22]. The fracture specimens have thickness $B = 13$ mm (0.5-T) and width $W = 26$ mm with crack length, a, to width ratio, $a/W = 0.5$. After fatigue pre-cracking, the specimens were side-grooved to a depth of 1 mm on each side to promote uniform crack growth over the thickness. The 0.5-T C(T) specimens were tested at room temperature using a direct current potential (DCP) method to measure the crack growth resistance for the material following the requirements of ASTM E1820 [24]. The material has 483 MPa yield stress (σ_{ys}) at room temperature (20°C) and relatively low hardening properties ($\sigma_{uts}/\sigma_{ys} \approx 1.24$), where σ_{uts} is the ultimate tensile strength [22]. Other mechanical properties for the material include Young's modulus, $E = 210$ GPa and Poisson's ratio, $\nu = 0.3$.

Consider first calibration of the GT parameters. Figure 4 shows the measured and predicted J-Δa curves for the 0.5-T C(T) specimen. Predicted R-curves are shown for three values of the initial volume fraction, $f_0 = 0.02$, 0.025 and 0.030 with the cell size taken as $D/2 = 100\ \mu$m and parameters $q_1 = 1.47$, $q_2 = 0.74$ [14]. For $f_0 = 0.02$, the predicted R-curve agrees well with the measured values for essentially the entire crack extension range. In contrast, the use of $f_0 = 0.025$ and 0.03 produces much lower resistance curve relative to the measured data. Consequently, the initial volume fraction $f_0 = 0.02$ is thus taken as the calibrated (plane-strain) value for the API 5L-X60 steel used in the study.

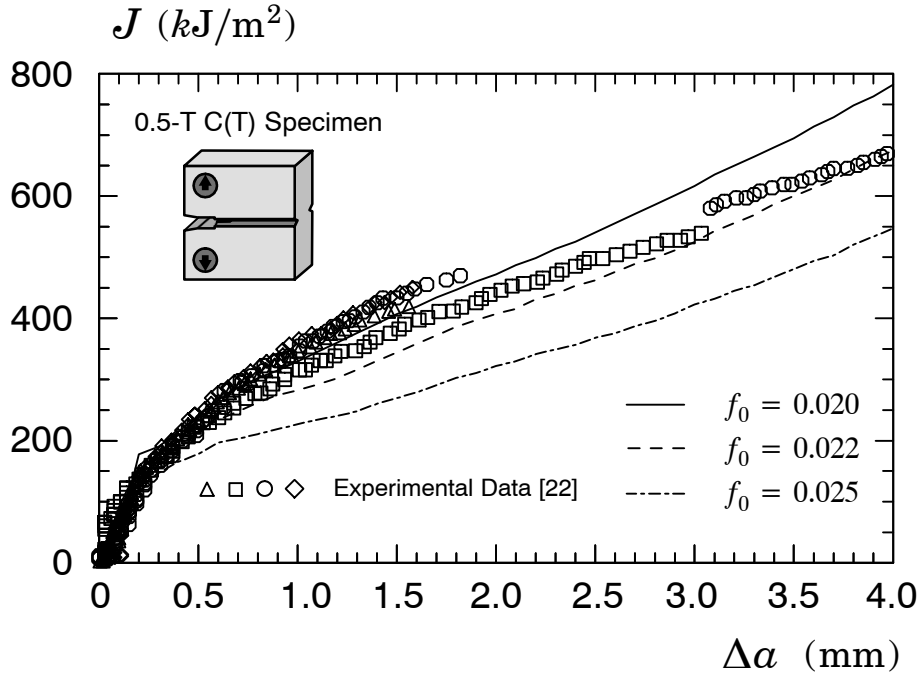

Figure 4 *Measured and predicted R-curve for side-grooved 0.5-T C(T) specimen of API 5L-X60 using the cell model.*

Consider next calibration of the CTOA parameters. Guided by numerical experiences, the CTOA-value at initiation is adopted as $\theta_I = 40°$. With the value of θ_I fixed, the calibration scheme then proceeds by finding the CTOA-value for crack propagation, θ_R, which provides the best fit to the measured R-curve. Figure 5 reveals that the predicted and measured R-curves are in excellent agreement for $\theta_R = 12.5°$.

4. APPLICATION TO BURST PRESSURE PREDICTIONS OF THIN-WALLED PIPELINES

4.1 Numerical Predictions of Ductile Crack Growth

To investigate the failure behavior of axially flawed pipelines, a series of full scale burst tests were performed on end-capped pipe specimens with external diameter, $D_e = 508$ mm (20 inches), wall thickness, $t = 15.8$ mm and length, $L = 3$ m (see [13]). These experimental tests included internal longitudinal surface cracks with different sizes measured by crack depth and crack length, $a \times 2c$, with a fixed $a/2c$-ratio of 0.05: 3×60 mm, 7×140 mm and 10×200 mm longitudinal flaws; hereafter,

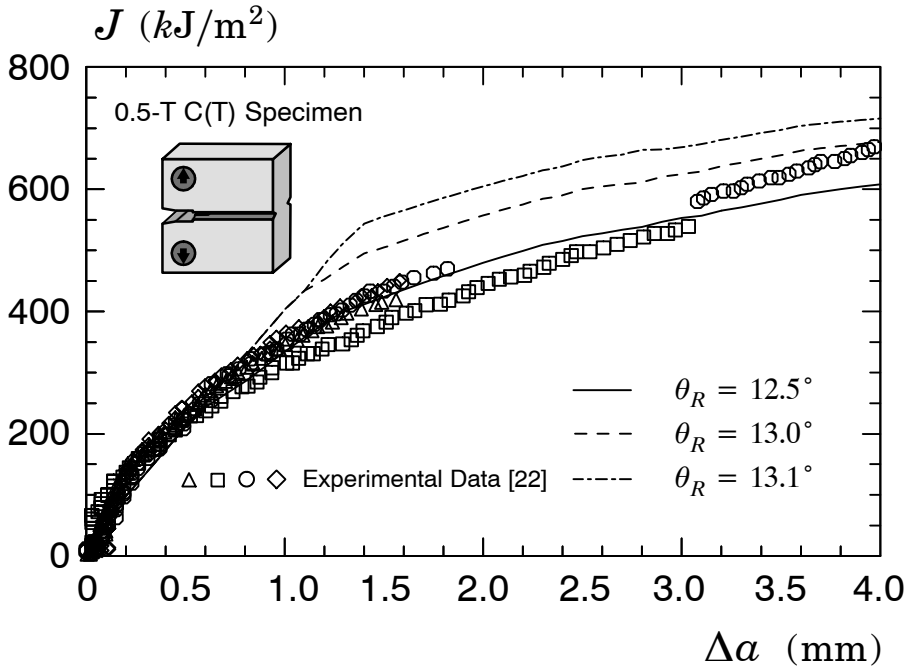

Figure 5 *Measured and predicted R-curve for side-grooved 0.5-T C(T) specimen of API 5L-X60 using the CTOA model.*

these pipe configurations are simply denoted as X60-P1, X60-P2 and X60-P3. During the loading of the pipes, ductile crack extension was monitored by using an ultrasonic pulse technique to measure the crack growth at the deepest point of the surface. [23]

Figure 6 displays the predicted evolution of crack growth with increased internal pressure for the analyzed pipe specimens based upon the GT model. In the present study, we adopt the cell parameters previously calibrated ($D/2 = 100\ \mu$m and $f_0 = 0.02$) as the material-specific parameters to predict the burst pressure for the pipe specimens. The numerical predictions based upon the cell model employ plane-strain finite element analyses of these specimens. To provide a simple comparison with the experimental data, this plot also includes the measured crack extension with increasing pressure for the pipe specimens X60-P1 (3mm crack depth) and X60-P2 (7 mm crack depth).

The general trend of crack growth evolution with increased pressure is correctly predicted for these pipe specimens, particularly for the X60-P2 configuration (7 mm crack depth). Here, we note that the numerical predictions provide slightly higher pressures values for a fixed amount of crack growth. Unfortunately, the comparisons of numerical predictions with experimental data for the pipe specimen X60-P3 (10 mm crack depth) cannot be made here as the amount of ductile tearing was not monitored for this case.

Figure 7 provides the predicted evolution of crack growth with increased internal pressure for the analyzed pipe specimens based upon plane-strain analyses using the CTOA model. Here, we adopt the CTOA parameters previously calibrated ($\theta_I = 40°$ and $\theta_R = 12.5°$) to predict the burst pressure for the pipe specimens. In contrast to the previous results, predictions of crack extension for the analyzed pipe specimens are in poor agreement with experimental results.

Figures 8(a-d) show the deformed profile for different load (pressure) levels, $P = 8$, 16, 24 and 27 MPa for the pipe specimen with 7 mm internal crack using the GT model. The pressure value $P = 27$ MPa marks the load almost immediately prior to pipe collapse (see Fig. 6). The predicted ductile behavior reproduces the essential features of the inward deflection (bulging) mechanism in the damaged (cracked) region of the pipe as the pressure increases. Moreover, these plots aid in understanding the behavior displayed in the previous Fig. 6 where there is a rapid increase in crack growth, Δa, for small changes in the internal pressure near the attainment of the maximum pressure in the experiments. Note the substantial change in the crack opening profiles for $P = 24$ and 27 MPa in comparison with the lower pressure levels. Following a transient period when the crack mouth opening remains relatively contained, the rapid development of the inward deflection (bulging) affects rather strongly the crack mouth opening and the amount of crack extension. The numerical results reported here for the pipe specimen with the 7 mm internal crack are essentially similar to corresponding results for other pipe specimens (to conserve space, they are not shown here).

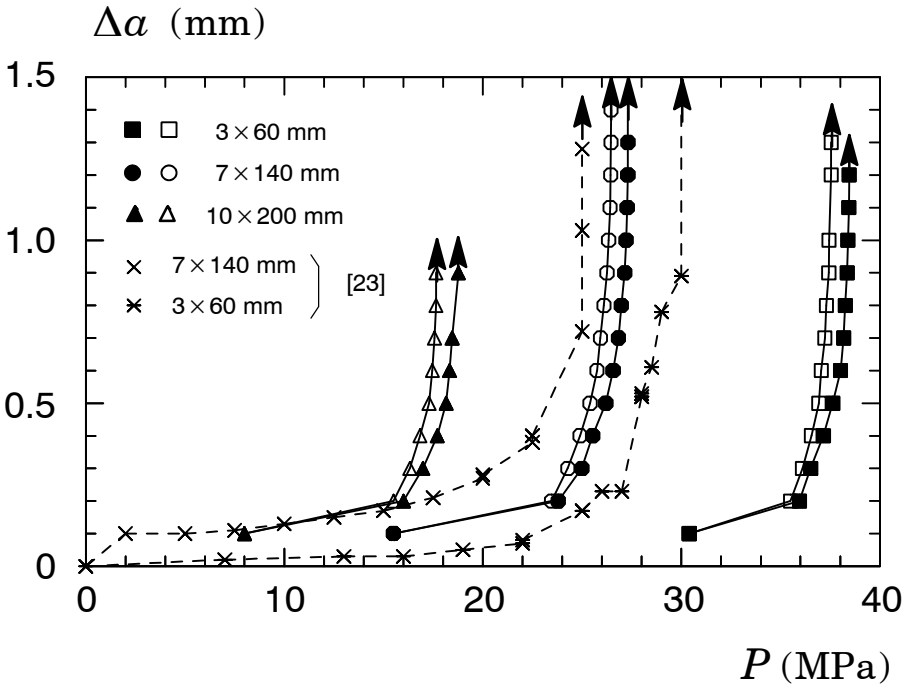

Figure 6 *Numerical prediction of crack growth in X60 pipe specimens based upon the GT model.*

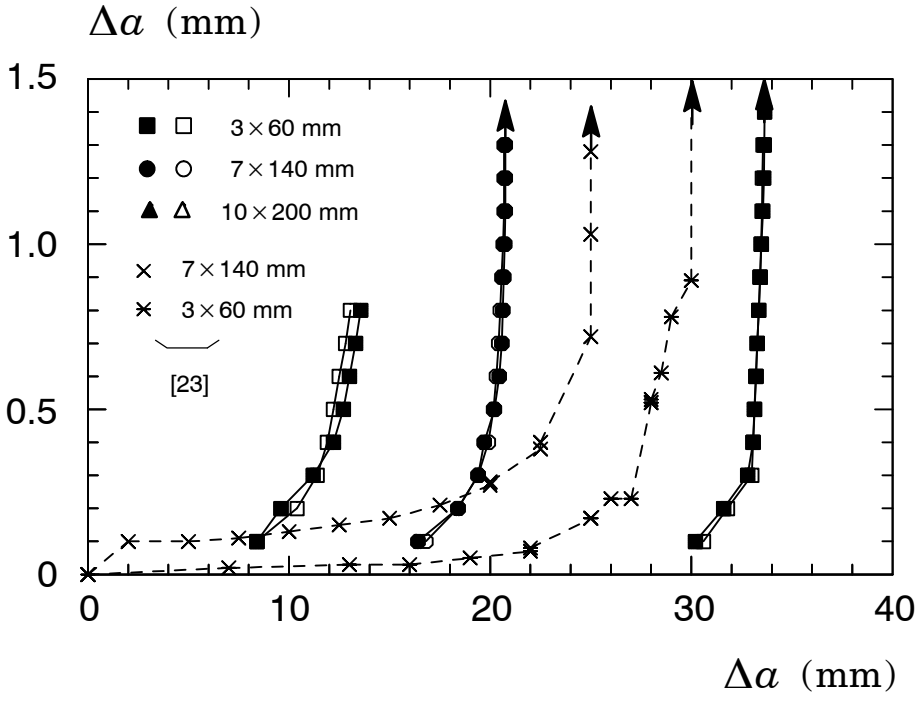

Figure 7 *Numerical prediction of crack growth in X60 pipe specimens based upon the CTOA model.*

4.2 Numerical Predictions of Burst Pressure

The evolution of ductile tearing with increased pressure displayed in previous Figs. 6 and 7 aids in establishing a simplified criterion to define the (predicted) burst pressure. Consider, for example, the pipe specimen X60-P2 in Fig. 6. Under

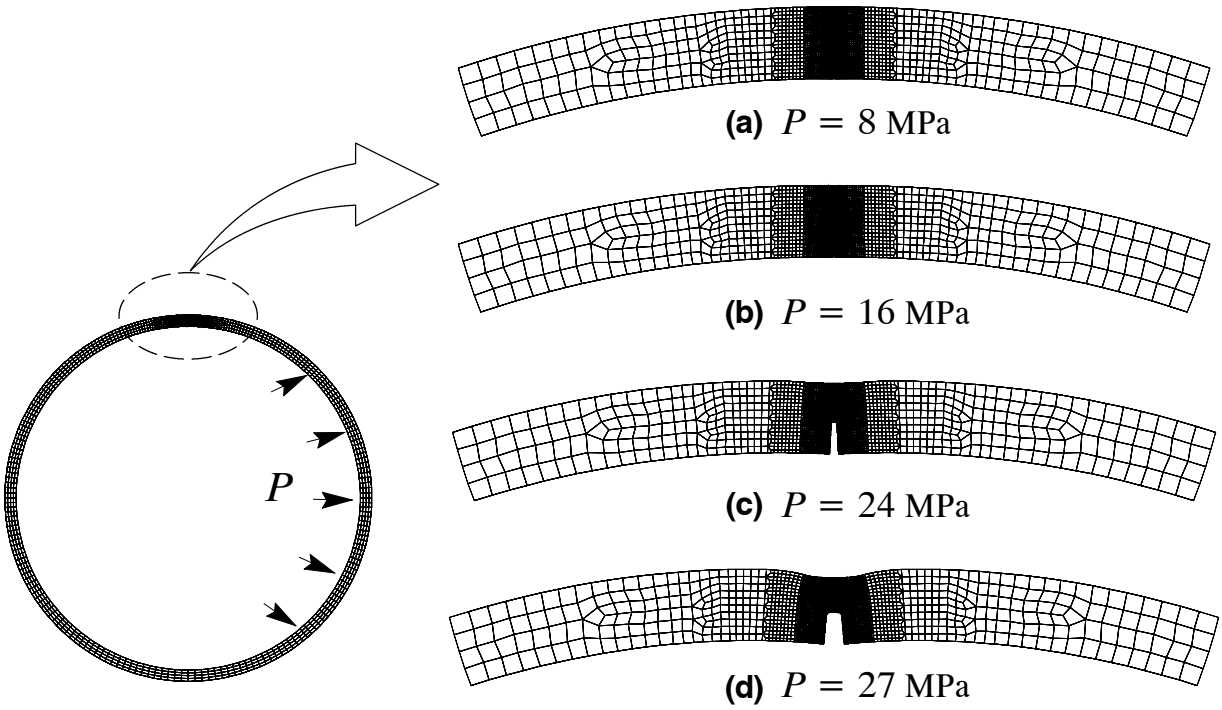

Figure 8 *Predicted evolution of bulging and crack opening for the pipe specimen with 7 × 140 mm internal crack at varying load (pressure) levels: (a) P = 8 MPa; (b) P = 16 MPa; (c) P = 24 MPa and d) P = 27 MPa.*

increased internal pressure, the rate of crack growth increases very slowly up to $P \approx 25$ MPa. This pressure value marks the beginning of very rapid ductile tearing with little increase in the applied pressure. After these pressure values (which are near the attainment of the maximum pressure observed in the tests), the load-carrying capacity of the remaining ligament cannot keep pace with the damage accumulation in the near-tip process zone (as characterized by the large number of damaged cell elements in the numerical model) so that an instability point is reached. Table 1 compares the experimental and predicted burst pressure for the tested X60 pipe specimens based upon the failure criterion just outlined. Predictions of the burst pressure based upon the cell model are in good agreement with measured values, particularly for the pipe specimen X60-P2 (7 mm crack depth). In contrast, the CTOA criterion provides a rather poor prediction of burst pressures for pipe specimens X60-P2 and X60-P3. Here, only the predicted burst pressure for the shallow crack pipe specimen (X60-P1 with 3 mm crack depth) agrees well with the corresponding measured value.

Table 1 *Comparison of measured and predicted burst pressure for X60 pipe specimens.*

Pipe Specimen	P_B Exp. (MPa)	P_B Pred. (MPa)	
		Cell Model	CTOA
X60-P1	33.0	38.3	33.2
X60-P2	27.5	27.3	20.5
X60-P3	22.0	18.8	13.4

4.3. Dependence of CTOA on Component Geometry

Application of the CTOA concept as a growth criterion in cracked structural components assumes independence of the CTOA during stable crack growth, on specimen geometry. A number of previous studies [16-21] consistently reveal a weak dependence of the critical CTOA on specimen size for thin panels and fracture specimens while others show a relatively

more pronounced dependence of θ_R on thicker specimen geometries. The relatively limited analyses available to describe crack growth resistance behavior for axially cracked pipelines based upon the CTOA underscores the need for further investigation.

Figure 9 shows the computed CTOA derived from plane-strain analyses conducted for the deeply cracked, 0.5-T C(T) fracture specimen and the pipe specimen with an external crack of 7×140 mm. The CTOA is directly computed from the deformation of the nodes at the crack tip derived from analyses using the cell model. After a transient stage of ductile tearing, $\Delta a \approx 0.5$ mm (where crack growth is driven by a nonconstat CTOA-value), crack extension for both configurations continues under a nearly constant CTOA-value. However, the strong dependence of CTOA during stable crack growth on specimen geometry is evident. Clearly, such behavior is associated with the dominant loading conditions in both crack configurations. The C(T) specimen is primarily a bend configuration whereas the cracked pipe under internal pressure is primarily subjected to strong membrane loading. Consequently, the assumption of a constant CTOA-value calibrated from using the C(T) fracture specimen accentuates the relatively poor agreement between measured and predicted burst pressures which is precisely the results shown in Fig. 9.

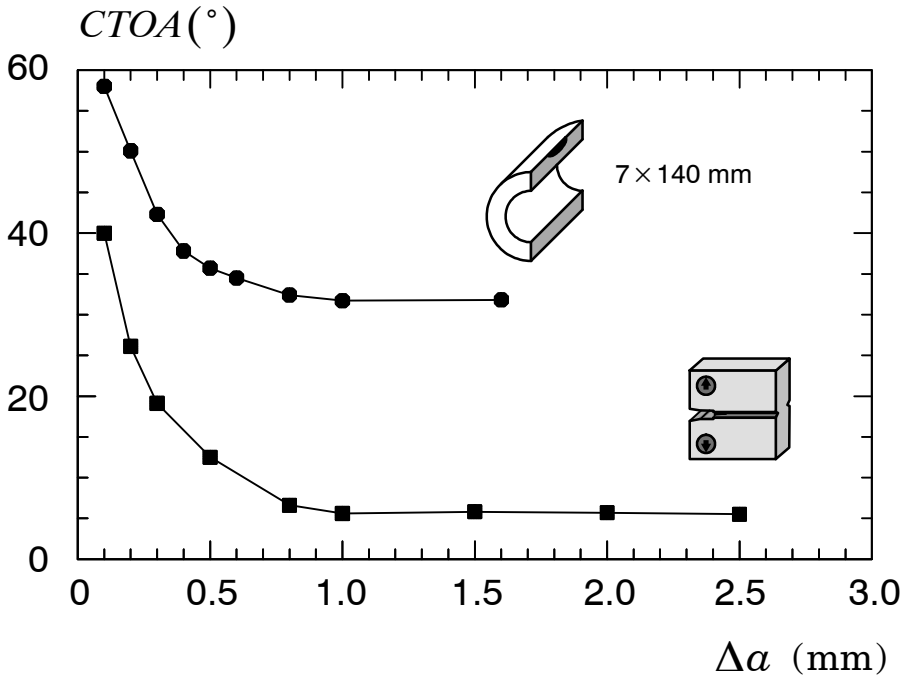

Figure 9 *Evolution of CTOA with crack extension for the deeply cracked 0.5-T C(T) specimen and the 7 mm precracked pipe specimen derived from the cell model.*

5. CONCLUDING REMARKS

This study described a micromechanics approach based upon the computational cell methodology incorporating the Gurson model and a deformation-based approach using the CTOA criterion to predict experimentally measured burst pressures for thin-walled gas pipeline containing longitudinal cracks. The analyses demonstrate the effectiveness and limitations of both approaches to describe crack growth response and to predict the burst pressure for the tested pipes. While the CTOA criterion still appears to have limited applicability to predict ductile cracking behavior for the pipe specimens, the cell model predictions of the ductile response for the precracked pipes show good agreement with experimentally measured burst pressures.

6. ACKNOWLEDGMENTS

This investigation was supported by Fundação de Amparo à Pesquisa do Estado de São Paulo (FAPESP) through Grant 03/02735-6. The authors acknowledge the Brazilian State Oil Company (Petrobrás) for making available the experimental data for the API 5L X60 pipeline steel plate and the burst pressure data. The authors also acknowledge the many useful discussions and contributions of José Claudio Guimarães Teixeira and Eduardo Hippert Jr. (CENPES-Petrobrás).

7. REFERENCES

[1] Kiefner, J. F., Maxey, W. A., Eiber, R. J. and Duffy, A. R. "Failure Stress Levels of Flaws in Pressurized Cylinders" in *Progress in Flaw Growth and Fracture Toughness Testing, ASTM STP 536*, American Society for Testing and Materials, Philadelphia, 1973, 461-481.

[2] Wilkowski, G., Stephens, G. Krishnaswamy, P., Leis, B. and Rudland, D. ''Progress in Development of Acceptance Criteria for Local Thinned Areas in Pipe and Piping Components." *Nuclear Engineering and Design*, 2000, (195):149-169.

[3] Hutchinson, J.W., ''Fundamentals of the Phenomenological Theory of Nonlinear Fracture Mechanics,'' *Journal of Applied Mechanics*, Vol. 50, pp. 1042–1051, 1983.

[4] American Petroleum Institute. "Fitness-for-Service", API RP-579-1 / ASME FFS-1, 2007.

[5] British Standard Institution. "Guide on Methods for Assessing the Acceptability of Flaws in Metallic Structures," BS7910, 2005.

[6] Gurson, A. L., ''Continuum Theory of Ductile Rupture by Void Nucleation and Growth: Part I - Yield Criteria and Flow Rules for Porous Ductile Media." *Journal of Engineering Materials and Technology*, Vol. 99, pp. 2-15, 1977.

[7] Tvergaard, V., ''Material Failure by Void Growth to Coalescence." *Advances in Applied Mechanics*, Vol. 27, pp. 83-151, 1990.

[8] Newman, J. C., James, M. A. and Zerbst, U., "A Review of the CTOA/CTOD Fracture Criterion", *Engineering Fracture Mechanics*, Vol. 70, pp.371-385, 2003.

[9] Gullerud, A. S., Dodds, R. H., Hampton, R. W. and Dawicke, D. S., "Three-Dimensional Modeling of Ductile Crack Growth in Thin Sheet Metals: Computational Aspects and Calidation", *Engineering Fracture Mechanics*, Vol. 63, pp.347-374, 1999.

[10] Xia, L. and Shih, C. F. ''Ductile Crack Growth - I. A Numerical Study Using Computational Cells with Microstructurally-Based Length Scales." *Journal of the Mechanics and Physics of Solids*, 1995, (43): 233-259.

[11] Ruggieri, C., Panontin, T. L. and Dodds, R. H. "Numerical Modeling of Ductile Crack Growth in 3-D Using Computational Cells." *International Journal of Fracture*, 1996, (82): 67-95.

[12] Koppenhoefer, K., Gullerud, A., Ruggieri, C., Dodds, R. and Healy, B., ''WARP3D: Dynamic Nonlinear Analysis of Solids Using a Preconditioned Conjugate Gradient Software Architecture", *Structural Research Series (SRS) 596*, UILU–ENG–94–2017, University of Illinois at Urbana–Champaign, 1994.

[13] Dotta, F. and Ruggieri, C., "Structural Integrity Assessments of High Pressure Pipelines with Axial Flaws Using a Micromechanics Model", *International Journal of Pressure Vessels and Piping*. Vol. 81, p. 761–770, 2004.

[14] Faleskog, J., and Shih, C.F., 'Cell Model for Nonlinear Fracture Analysis - I: Micromechanics Calibration." *International Journal of Fracture*, Vol. 89, pp. 355-373, 1998.

[15] Ruggieri, C. and Hippert, E. "Cell Model Predictions of Ductile Fracture in Damaged Pipelines" in *Fatigue and Fracture Mechanics:33rd Volune, ASTM STP 1417*, W. G. Reuter and R. S. Piascik, Eds., American Society for Testing and Materials, Philadelphia, pp. 291-317, 2002.

[16] Shih, C. F., de Lorenzi, H. G. and Andrews, W. R., "Studies on Crack Initiation and Stable Crack Growth," *Elastic-Plastic Fracture, ASTM STP 668*, J. D. Landes, et al. Eds., American Society for Testing and Materials, Philadelphia, pp. 65-120, 1979.

[17] Newman Jr., J. C., "An Elastic-Plastic Finite Element Analysis of Crack Initiation, Stable Crack Growth and Instability," *Fracture Mechanics, ASTM STP 833*, R. J. Stanford Eds., American Society for Testing and Materials, Philadelphia, pp. 93-117, 1984.

[18] Newman Jr., J. C., Booth, B. C. and Shivakumar, K. N., "An Elastic-Plastic Finite Element Analysis of the J-Resistance Curve Using a CTOD Criterion," *Fracture Mechanics, ASTM STP 945*, R. J. Stanford Eds., American Society for Testing and Materials, Philadelphia, pp. 665-685, 1988.

[19] Gullerud, A. S., Dodds, R. H., Hampton, R. W. and Dawicke, D. S. "Three-Dimensional Modeling of Ductile Crack Growth in Thin Sheet Metals: Computational Aspects and Validation" *Engineering Fracture Mechanics*, Vo. 63, pp. 347-374, 1999.

[20] Deng, X. and Newman Jr., J. C., "A Study of Some Issues in Stable Tearing Crack Growth Simulations," *Engineering Fracture Mechanics*, Vo. 64, pp. 291-304, 1999.

[21] Newman Jr., J. C., James, M. A. and Zerbst, U., "A Review of the CTOA/CTOD Criterion," *Engineering Fracture Mechanics*, Vo. 70, pp. 371-385, 2003.

[22] Silva, M. S. "Fracture Toughness and R-Curve Measurements for an API X60 Pipeline Steel Using a Direct Current Potential Technique." *M.Sc. Thesis*. Faculty of Engineering (COPPE), Federal University of Rio de Janeiro, 2002 (in Portuguese).

[23] Petrobrás, "Ultrasonic Measurements in Burst Pressure Tests for a 20" O.D. API Grade 5L X60 Pipelines." *Private Report*, 2002 (in Portuguese).

[24] American Society for Testing and Materials, "Standard Test Method for Measurement of Fracture Toughness", ASTM E1820, 2008.

8. RESPONSIBILITY NOTICE

The authors are the only responsible for the printed material included in this paper.